Teramoto et al. Earth, Planets and Space (2016) 68:22
DOI 10.1186/s40623-016-0397-1

Earth, Planets and Space
a SpringerOpen Journal

FULL PAPER Open Access

Latitudinal dependence on the frequency of Pi2 pulsations near the plasmapause using THEMIS satellites and Asian-Oceanian SuperDARN radars

Mariko Teramoto[1*], Nozomu Nishitani[2], Yukitoshi Nishimura[3] and Tsutomu Nagatsuma[4]

Abstract

We herein describe a harmonic Pi2 wave that started at 09:12 UT on August 19, 2010, with data that were obtained simultaneously at 19:00–20:00 MLT by three mid-latitude Asian-Oceanian Super Dual Auroral Radar Network (SuperDARN) radars (Unwin, Tiger, and Hokkaido radars), three Time History of Events and Macroscale Interactions during Substorms (THEMIS) satellites (THEMIS A, THEMIS D, and THEMIS E), and ground-based magnetometers at low and high latitudes. All THEMIS satellites, which were located in the plasmasphere, observed Pi2 pulsations dominantly in the magnetic compressional ($B_{//}$) and electric azimuthal (E_A) components, i.e., the fast-mode component. The spectrum of Pi2 pulsations in the $B_{//}$ and E_A components contained two spectral peaks at approximately 12 to 14 mHz (f_1, fundamental) and 23 to 25 mHz (f_2, second harmonic). The Poynting flux derived from the electric and magnetic fields indicated that these pulsations were waves propagating earthward and duskward. Doppler variations (V) from the 6-s or 8-s resolution camping beams of the Tiger and Unwin SuperDARN radars, which are associated with Pi2 pulsations in the eastward electric field component in the ionosphere, observed Pi2 pulsations within and near the footprint of the plasmapause, whose location was estimated by the THEMIS satellites. The latitudinal profile of f_2 power normalized by f_1 power for Doppler velocities indicated that the enhancement of the normalized f_2 power was the largest near the plasmapause at an altitude-adjusted corrected geomagnetic (AACGM) latitude of 60° to 65°. Based on these features, we suggest that compressional waves propagate duskward away from the midnight sector, where the harmonic cavity mode is generated.

Keywords: Pi2 pulsations near the plasmapause, Multipoint observations, Mid-latitude SuperDARN radars, THEMIS satellites

Introduction

Pi2 pulsations with a period of 40 to 150 s and damping waveforms usually occur at the onset of a substorm (Keiling and Takahashi 2011). These pulsations can be observed over a wide latitudinal range on the ground within the nightside sector. Ground magnetometer data along one meridian on the nightside have shown that Pi2 pulsations have a common period at latitudes lower than the plasmapause position. The longitudinal profiles of phase and amplitude show an H-component 180° phase shift across the plasmapause position and an H-component amplitude maximum equatorward of the plasmapause position (Yeoman and Orr 1989). Observations taken with ground magnetometers on the nightside have revealed that the plasmapause, where the phase and amplitude change, is the transition region between high- and low-latitude Pi2 pulsations.

Cavity mode resonance (Saito and Matsushita 1968) in the plasmasphere has been proposed as a possible generation mechanism for the mid- and low-latitude Pi2 pulsations. This mode is excited by impulsive fast-mode waves, which propagate earthward in the magnetic equatorial plane from the magnetotail at the substorm onset. After reaching the plasmasphere, the

* Correspondence: teramoto@stp.isas.jaxa.jp
[1]Institute of Space and Astronautical Science, Japan Aerospace Exploration Agency, 3-1-1 Yoshinodai, Chuo-ku, Sagamihara, Kanagawa 252-5210, Japan
Full list of author information is available at the end of the article

fast-mode waves propagate back and forth between the inner and outer boundaries (i.e., the ionosphere and the plasmapause) and establish standing waves in the plasmasphere. In this scenario, the plasmapause plays an important role as the outer boundary in establishing standing waves in the plasmasphere. By using the magnetic field data from the equatorial orbiting Active Magnetospheric Particle Tracer Explorer (AMPTE)/Charge Composition Explorer (CCE) satellite and data from the Kakioka (KAK), Japan, ground station located at $L = 1.23$, Takahashi et al. (1995) statistically investigated the spatial characteristics of Pi2 pulsations in the inner magnetosphere and found that Pi2 pulsations in the compressional ($B_{//}$) and radial (B_R) components, which have high coherence with those observed in the northward (H) component on the ground on the nightside, are primarily observed on the nightside at $L < 4$. They assumed cavity mode resonance within the plasmapause, which was located at $L \cong 4$ in their observations. To clarify the relationships between Pi2 pulsations and the plasmapause in more detail, Takahashi et al. (2003a) studied the radial structure of the amplitude and cross-phase between Pi2 pulsations in the inner magnetosphere and on the ground as well as their dependence on the plasmapause position by using electron density and electric and magnetic field data obtained from the Combined Release and Radiation Effects Satellite (CRRES). They showed that the E_A-H cross-phase is approximately 90° at all distances in the plasmasphere even near the plasmapause, whereas the $B_{//}$-H cross-phase clusters at either 0° or 180° near the plasmapause. These radial properties of amplitude and cross-phase imply that the fundamental cavity mode resonance is excited in the plasmasphere.

The power spectrum of ground Pi2 pulsations at low latitudes often contains up to four harmonics (Lin et al. 1991; Nosé 1999; Cheng et al. 2000). These harmonic Pi2 pulsations have been attributed to the cavity mode resonance with higher harmonics. Satellites orbiting in the inner magnetosphere can detect the signatures of multifrequency Pi2 pulsations in the electric and magnetic fields (Denton et al. 2002). The nodal structure for second-harmonic Pi2 pulsations was investigated in detail by Takahashi et al. (2003b) who employed the electric and magnetic field data obtained by the CRRES and ground magnetic field data at KAK. They found that the CRRES spectra of Pi2 pulsations in the E_A and B_Z components have a single peak at the fundamental (f_1) and second (f_2) frequencies, respectively, whereas those of Pi2 pulsations in the H component at KAK exhibited a peak at both f_1 and f_2. They also showed the phase relationship among the field components. At f_1, the phase of E_A relative to H was −90°, and the phase of $B_{//}$ relative to H was −180° at f_2. The spectral and phase features of the electric and magnetic fields from the satellite provide evidence for harmonic cavity mode resonance in the plasmasphere. The radial profile of the harmonic cavity mode resonance was shown by Luo et al. (2011) who used data from the Time History of Events and Macroscale Interactions during Substorms (THEMIS) multisatellite observations and low-latitude ground observations, which were performed at approximately the same longitude on the nightside. These data also provide evidence for the harmonic cavity mode resonance, which is confined in the plasmasphere.

Investigating the spatial structure of ultra low-frequency (ULF) waves in the electric field of the ionosphere by using the high-frequency (HF) Super Dual Auroral Radar Network (SuperDARN) radars is possible (Ponomarenko et al. 2003). Over large areas, these radars emit oblique HF signals and receive ionospheric scatter (IS) and ground/sea scatter (GS) echoes, which are backscattered from decameter-scale electron density irregularities in the E or F region ionosphere and from irregularities on the ground or sea surface, respectively. Gjerloev et al. (2007) first reported that sub-auroral Pi2 pulsations detected by the Wallops radar were highly correlated with those in the magnetic field from a nearby ground station. Modeling of the event indicated that the predominantly shear Alfvén mode from an altitude of 1000 km provides amplitudes and phase relations that agree with the observations. By using data obtained by the Blackstone SuperDARN radar and nearby ground magnetometers, which were located in the pre-midnight sector of the sub-auroral region, Frissell et al. (2011) studied the fine spatial and temporal details of radar data at the ionospheric projection of the plasmapause and found evidence of field-line compressions. Comparing these Pi2 pulsations and the earthward-moving busty bulk flows (BBFs) observed by the THEMIS E and D satellites, Frissell et al. (2011) concluded that these compressions provide support for a BBF-driven Pi2 model, which is an alternative generation mechanism for mid- and low-latitude Pi2 pulsations that was first proposed by Kepko and Kivelson (1999). In the BBF-driven Pi2 model, quasi-periodical braking of earthward-flowing BBFs from the magnetotail produces compressional waves in the inner magnetosphere, which directly drive Pi2 pulsations from high to low latitudes. These compression features can be detected only by radars that provide significantly better spatial resolution of the range gate cell along the line of sight.

Although radar observations are capable of investigating the spatial structure of Pi2 pulsations at mid latitudes (36°–60°), only a few studies have investigated Pi2 pulsations by using the SuperDARN radars at mid latitudes (Ponomarenko et al. 2003; Gjerloev et al. 2007; Frissell et al. 2011; Teramoto et al. 2014). To investigate generation mechanisms of Pi2 pulsations, multipoint observations are

needed because Pi2 pulsations are globally excited in the mid and low latitudes. In particular, a comprehensive survey of Pi2 pulsations near the plasmapause is important because the plasmapause is the transitional region for the cavity mode resonance (Yeoman et al. 1991). In this study, we focus on a mid-latitude Pi2 pulsation event that occurred around the plasmapause at 09:12 UT on August 19, 2010, and the event was evaluated with data that were obtained simultaneously on the duskside by three THEMIS satellites (THEMIS A (THA), THEMIS D (THD), and THEMIS E (THE)) as well as the mid-latitude Unwin, Tiger, and Hokkaido SuperDARN radars and ground magnetometer stations. Based on these observations, we compared the spectral properties of Pi2 pulsations and found that they had both fundamental and second-harmonic frequencies. The enhancement of the power spectral density of second harmonics was radially localized in a small area at mid latitudes near the plasmapause. We will show that the Pi2 pulsations were excited by propagating fast-mode waves, which were generated by the cavity mode resonance on the nightside with a harmonic structure.

The remainder of this paper is organized as follows. In the "Data sets" section, we present the data sets used in this study. In the "Observations" section, we present the results for the Pi2 pulsations that occurred at the substorm onset on August 19, 2010. We then discuss the generation mechanisms of this event in the "Discussion" section and present a summary in the "Summary" section.

Data sets

The data used in this study were obtained by three THEMIS satellites (THA, THD, and THE) (Angelopoulos et al. 2008); three mid-latitude SuperDARN radars (Greenwald et al. 1995; Chisham et al. 2007) that are installed in Hokkaido, Japan (Hokkaido (HOK) radar, altitude-adjusted corrected geomagnetic (AACGM) coordinates 36.5°, −145.3°), Unwin, New Zealand (Unwin (UNW) radar, AACGM coordinates −54.4°, −106.3°), and Tasmania, Australia (Tiger (TIG) radar, AACGM coordinates 36.5°, −145.3°); and from ground stations in East Asia and Oceania, which were located approximately along the 210° magnetic meridian. Figure 1 shows the field of view of the three SuperDARN radars, the footprints of the THEMIS satellites, and the locations of ground stations on an AACGM map (Baker and Wing 1989). The footprints of the satellites were mapped at a height of 100 km in the ionosphere along the Earth's magnetic field by using the Tsyganenko 96 model (see Tsyganenko 1996). The field of view of the radars, the footprints of the THEMIS satellites, and the ground stations were located on the duskside at 19:00–21:00 MLT; the substorm started at 09:12 UT on August 19, 2010.

THEMIS satellites

The THEMIS satellites, specifically, five satellites (THEMIS A through THEMIS E) with elliptic orbits, were launched on February 17, 2007. The mission of these satellites is comprised of several stages with different orbital configurations. In the present study, Pi2 pulsations were observed at

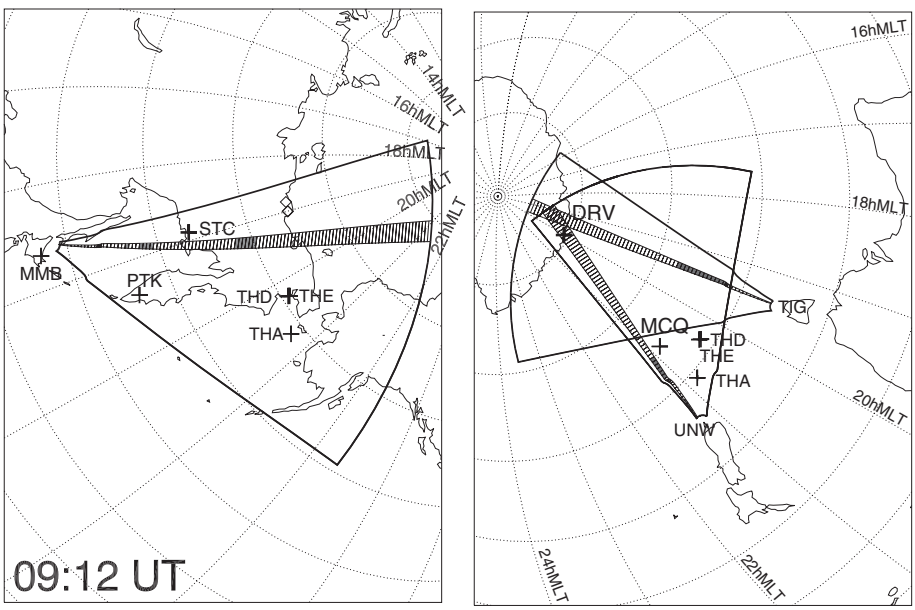

Fig. 1 Field of view of the Hokkaido, Tiger, and Unwin radars, the footprints of the THEMIS A, D, and E satellites at an altitude of 100 km, and geomagnetic stations at 09:12 UT on August 19, 2010. *Shaded regions* of the field of view indicate locations of echoes with Pi2 frequencies. Satellite footprints were calculated by using the T96 geomagnetic field model

stage 12 of the "Dusk Phase." During this stage, the apogee (perigee) of three satellites, namely, THA, THD, and THE, was approximately 12 R_E (1.5 R_E) and was located on the dusk (dawn)side of the magnetosphere.

We used the magnetic and electric field data obtained by a fluxgate magnetometer (FGM) and an electric field instrument (EFI) with a 3-s spin period resolution that were carried onboard the THEMIS satellites for the data analyses. The electric field data used in this study is the spin-axis component, which was derived by assuming that no electric field exists along the background magnetic field ($\mathbf{E} \cdot \mathbf{B} = 0$). By using the International Geomagnetic Reference Field (IGRF) model, the coordinates of the magnetic and electric field data were converted to the local magnetic (LMG) coordinate system, where $\boldsymbol{e}_{//}$ is a unit vector parallel to the model magnetic field, $\boldsymbol{e}_A$ pointing eastward is the unit azimuthal component perpendicular to the $\boldsymbol{e}_{//}$ vector and the position vector of the satellite, and $\boldsymbol{e}_R$ pointing radially outward is the unit radial component parallel to $\boldsymbol{e}_A \times \boldsymbol{e}_{//}$.

SuperDARN radars

The SuperDARN is operated as an international radar network project for investigating the upper atmosphere and ionosphere, and in 2015, the network was comprised of 22 radar sites in the Northern Hemisphere and 11 radar sites in the Southern Hemisphere. In the standard operating mode, each radar sweeps through 16 beam directions that are azimuthally separated by 3.24° with a total azimuthal field of view of 52°. Each beam is comprised of 75 or 110 range gates, where the first gate is 180 km in length and the others are 45 km in length. The SuperDARN radars transmit the HF signals with oblique incidence and receive the HF signals that are backscattered by small-scale ionospheric irregularities at the E or F region height with Doppler shifts or by the sea/ground surface.

A number of operating modes are possible with the SuperDARN radar. Normally, the SuperDARN radar operates once every minute during the normalscan mode with all beams. In this study, we used the Doppler velocity measurements taken during the themisscan mode by the three mid-latitude SuperDARN radars. When the themisscan mode is operated, the SuperDARN radar provides high temporal resolutions for one single beam, which is called the camping beam. The camping beam of beam 4 (beams 14 and 4) at the HOK (UNW and TIG) radar is sampled every 8 (6) seconds, which is suitable for analyzing Pi2 pulsations with periods of 40–150 s. The locations of the camping beams are shown as meshed areas in Fig. 1.

The electric field of ULF waves at ionospheric height can be detected as Doppler velocity variations in both IS and GS echoes. In the IS echoes, the radar measures the line-of-sight component of the $\mathbf{E} \times \mathbf{B}$ drift velocities, which are produced by the ULF electric field $\boldsymbol{E}$ in the background magnetic field $\boldsymbol{B}_0$. The east–west electric field component primarily affects the Doppler velocity variations in the IS echoes of the camping beams at the HOK, UNW, and TIG radars because all camping beams point approximately toward the geomagnetic poles. According to previous studies (e.g., Bourdillon et al. 1989), ULF variations in the Doppler velocities of sea scatter echoes are primarily the result of vertical motions due to $\mathbf{E} \times \mathbf{B}$ drift.

Ground magnetometers

To compare the variation of the Doppler velocities with ground Pi2 pulsations, we used the geomagnetic field data obtained by the five ground stations listed in Table 1. In this paper, three-letter codes were used to identify the ground stations. Two of the five stations, namely, Macquarie (MCQ) and Dumont d'Urville (DRV), were located in the Southern Hemisphere. All geomagnetic field data had time resolutions of 1 s. The H (D) component is northward (eastward) in the geographic coordinates.

Observations

Magnetospheric conditions

The event which we focused on had a 3-h Kp index of less than 1+ all day before August 19, 2010, which indicates that the magnetosphere remained in a quiet and steady state. Figure 2a shows the provisional auroral electrojet (AL) index from 09:00 to 10:00 UT on August 19, 2010. The decrease from −70 to −250 nT in the AL index indicates that the substorm onset occurred at 09:12 UT, as represented by the vertical dashed line. To show that Pi2 pulsations occurred globally at low latitudes, Fig. 2b illustrates the time series plots of the H component at Honolulu (HON) and Memanbetsu (MMB) at low latitudes during the interval between 09:00 and 10:00 UT. The substorm onset can also be identified by the positive bay in the geomagnetic field data at HON,

Table 1 Coordinates of ground stations

Station name	Geog.		Mag.		MLT (hour) at 09:12 UT
	Lat. (deg)	E Long. (deg)	Lat.	Long.	
STC (Magadan)	59.97	150.86	53.6	218.9	18:54
PTK (St. Palatunka)	52.94	158.25	46.2	226.2	19:23
MMB (Memanbetsu)	43.92	144.20	37.1	215.5	18:32
MCQ (Macquarie)	−54.50	158.95	−64.5	248.1	20:50
DRV (Dumont d'Urville)	−66.67	140.01	−80.6	235.8	20:01

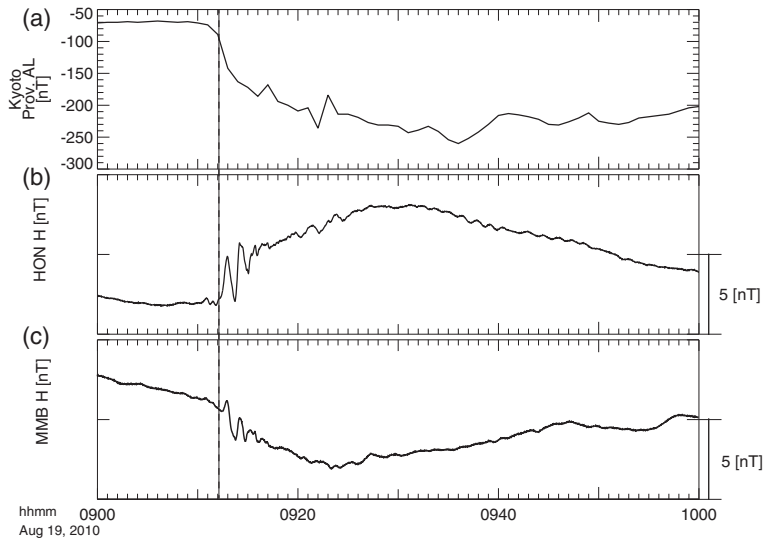

Fig 2 **a** Auroral electrojet AL index, **b** Honolulu (*HON*) data, and **c** Memanbetsu (*MMB*) data for the *H* component from 09:00 to 10:00 UT on August 19, 2010. The *vertical dashed lines* indicate the substorm onset at 09:12 UT on August 19, 2010

which occurred at midnight. Clear Pi2 pulsations appeared simultaneously at the substorm onset at HON and MMB.

The electric field experiments on the THEMIS satellites allowed us to estimate the electron number densities and to determine the location of the plasmapause. Figure 3 shows the electron number density derived from the THEMIS spacecraft potential data plotted as a function of an AACGM latitude in the ionosphere at a height of 100 km, which was determined by use of the Tsyganenko 96 model. The electron number density increased steeply around 65.5° AACGM latitude, which was the location of the plasmapause. During the time intervals of Pi2 pulsations observed by the satellites, which are indicated by the horizontal lines in Fig. 3, all three satellites were located in the plasmasphere.

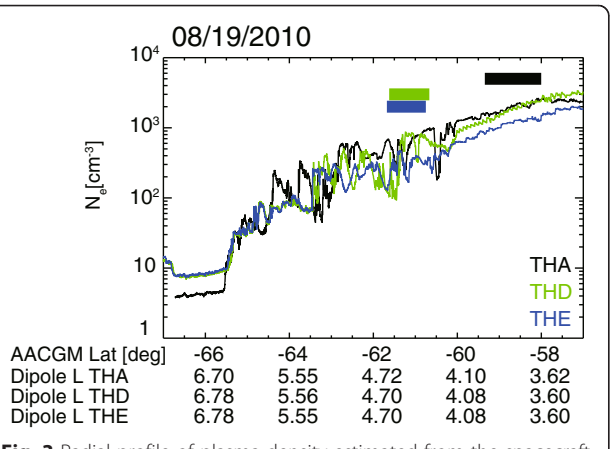

Fig. 3 Radial profile of plasma density estimated from the spacecraft potential data of THEMIS on August 19, 2010. Horizontal bars indicate intervals of Pi2 pulsations observed by the THEMIS satellites

Satellite observations of Pi2 pulsations

Figure 4c shows the perturbations of the electric and magnetic fields from the satellites, which were observed simultaneously at the low-latitude MMB station when THA (THD and THE) was (were) located in the Northern (Southern) Hemisphere pre-midnight sector, as shown in Fig. 4a, b at 09:12 UT. The THD and THE were very close to each other during the Pi2 pulsations. For all three satellites, the E_R, E_A, and $B_{//}$ components exhibited oscillations in the Pi2 frequency band with slightly different waveforms from the Pi2 pulsations in the *H* component at MMB. The Pi2 pulsation did not appear clearly in the B_R and B_A components. Note that regular oscillations with periods of 1 min in the B_A component were artificial. The E_R, E_A, and $B_{//}$ components oscillated with periods of 40 and 70 s throughout the event, whereas Pi2 pulsations at MMB oscillated with dominant periods of 70 s. The amplitude of the 40-s oscillations was much smaller than that of the 70-s oscillations. Oscillations in the $B_{//}$ and E_R components were in-phase relative to those on the ground, whereas the Pi2 pulsations in the E_A component had an out-of-phase relation with those on the ground. These phase characteristics indicate that the Pi2 pulsations from satellites were not standing waves but rather propagating waves.

Figure 5 shows the spectral properties of the event. The electric and magnetic field data from satellites were linearly interpolated and resampled at the same 1-s time rate as the geomagnetic field data. After subtracting 300-s boxcar data from the original data to remove long-term variations, which were defined as d*H*, d*B*, and d*E*, a fast Fourier transform (FFT) was applied to the residual d*H*, d*B*, and d*E* in the time interval from 09:11 to 09:19 UT

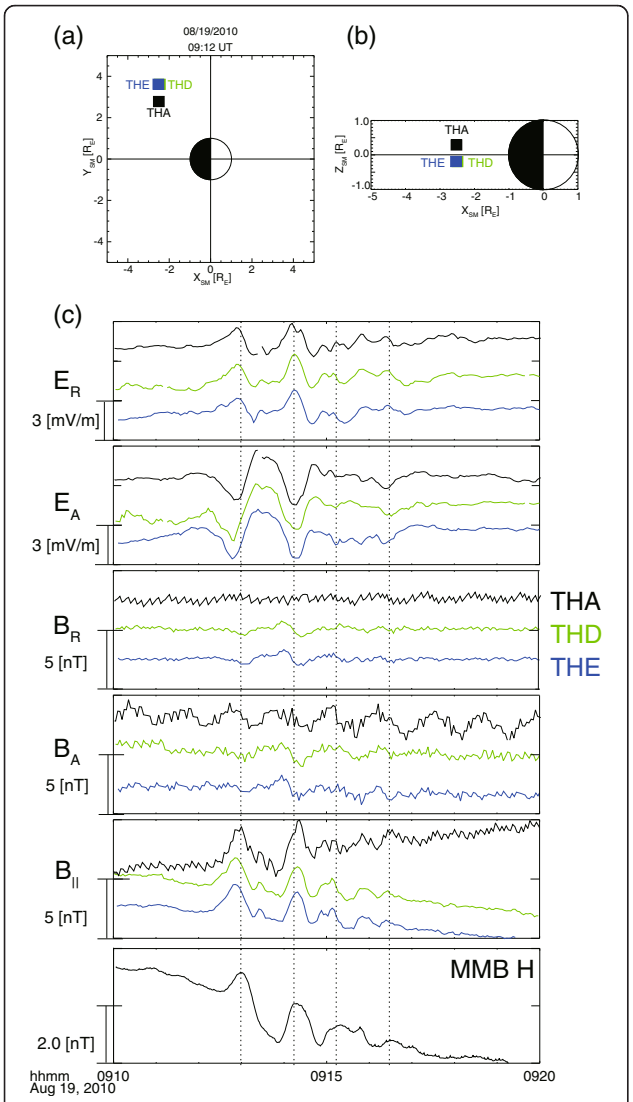

Fig. 4 Locations of the THEMIS satellites at 09:12 UT on August 19, 2010, in **a** the *X-Y* plane and **b** the *X-Z* plane in the solar magnetic (SM) coordinate system. **c** Time series of the electric field and magnetic field data from THEMIS and the geomagnetic field in the *H* component of MMB

(512 data points), and three-point smoothing was conducted in the frequency domain, thus providing a Nyquist frequency of 500 mHz and a frequency resolution of 1.9 mHz. The upper left, middle, and right panels of Fig. 5 indicate the spectral properties of the Pi2 pulsations in the electric and magnetic fields observed by the THA, THD, and THE satellites, respectively. The power spectral densities for the dE_A, dE_R, and $dB_{//}$ variations from the satellites and the dH variations at MMB, which represent $S^{(dEA)}(f)$, $S^{(dER)}(f)$, $S^{(dB//)}(f)$, and $S^{(dH)}(f)$, exhibited clear peaks around 12 to 14 (f_1) mHz. At 23 to 25 (f_2) mHz, $S^{(dEA)}$, $S^{(dER)}$, $S^{(dB//)}$, and $S^{(dH)}$ had their second highest peaks. The total $S(f_2)/S(f_1)$ power ratio for the dE_A, dE_R, $dB_{//}$, and dH components was lower than 0.7. At both f_1 and f_2, the dE_A–dH, dE_R–dH, and $dB_{//}$–dH coherences were nearly perfect (approximately 1.0), and the cross-phase spectra showed that dH was in-phase with $dB_{//}$ and dE_R was out of phase with dE_A.

In order to identify the direction of the wave energy propagation, we calculated the Poynting flux **P** by using the following formula:

$$\mathbf{P} = \frac{d\mathbf{E} \times d\mathbf{B}}{\mu_0}$$

Figure 6 shows the Poynting flux in the radial, azimuthal, and parallel components (positive radially outward, duskward, and northward, respectively). The transverse components exhibited non-zero mean values during the Pi2 interval. The negative P_A and P_R components imply that wave energy propagated westward and earthward. These features were inconsistent with the cavity mode model, in which the Poynting flux in the radial component had a mean value close to zero because the cavity mode consisted of standing fast-mode waves. The amplitude of the Poynting flux in the parallel component was smaller than that in the transverse components. The sign of $P_{//}$ from THA was positive, whereas the signs of $P_{//}$ from THE and THD were negative. This means that the electromagnetic energy flux was directed away from the magnetic equator and toward both hemispheres.

SuperDARN observations

Figure 7 shows the time series plots of the line-of-sight Doppler velocities obtained with the UNW radar (beam 14, ranges of 3–5 and 14–22 (Fig. 7a)); with the TIG radar (beam 4, range of 13–27 (Fig. 7b)); and with the HOK radar (beam 4, ranges of 21–29 and 53–57 (Fig. 7c)) on August 19, 2010, at 09:10–09:20 UT. The black arrows indicate the plasmapause locations, which were estimated by the electron number density from the THEMIS satellites, as shown in Fig. 3. The plasmapause was located between the range of 21 and 22 for the UNW, and it occurred at latitudes higher than the observation points of the HOK and UNW radars. Furthermore, we present a time series plot of the geomagnetic field variations in the dH component at MCQ in the bottom panels of the UNW and TIG observations and those in the dH component at St. Palatunka (PTK) in the bottom panels of the HOK observations. These geomagnetic observations were made at almost the same latitudes as the observation points in the field of view of each radar. At lower latitudes, the amplitudes of Doppler velocity variations from the HOK radar at lower latitudes were smaller than those at higher latitudes. The periods of Doppler velocity variations from the HOK radar at ranges 53–56 were almost identical to those of the Pi2 pulsations

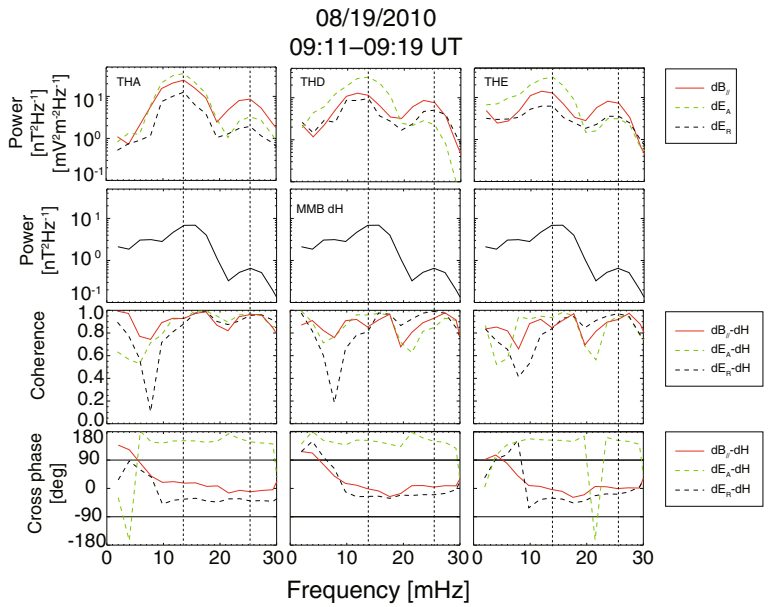

Fig. 5 Spectral properties of the d$B_{//}$, dE_A, and dE_R components for the THEMIS satellites and the dH component for MMB. (*top*) Power spectral density. (*middle*) Coherence. (*bottom*) Cross-phase given in degrees

in the dH component at PTK with a 180° phase difference. Data from the UNW radar showed that the periods of Doppler variations were much shorter than those of the Pi2 pulsation in the dH component at MCQ and the largest amplitude was recorded around a range of 16. At higher ranges (14–22), the waveforms of Doppler variations from the UNW radar were almost identical. In the Doppler velocities from the TIG radar, the periods of the variations were identical at all ranges between 09:13 and 09:15 UT, whereas the periods at higher latitudes (range of 19–27), which were located near or outside the plasmapause, were longer than those at lower latitudes

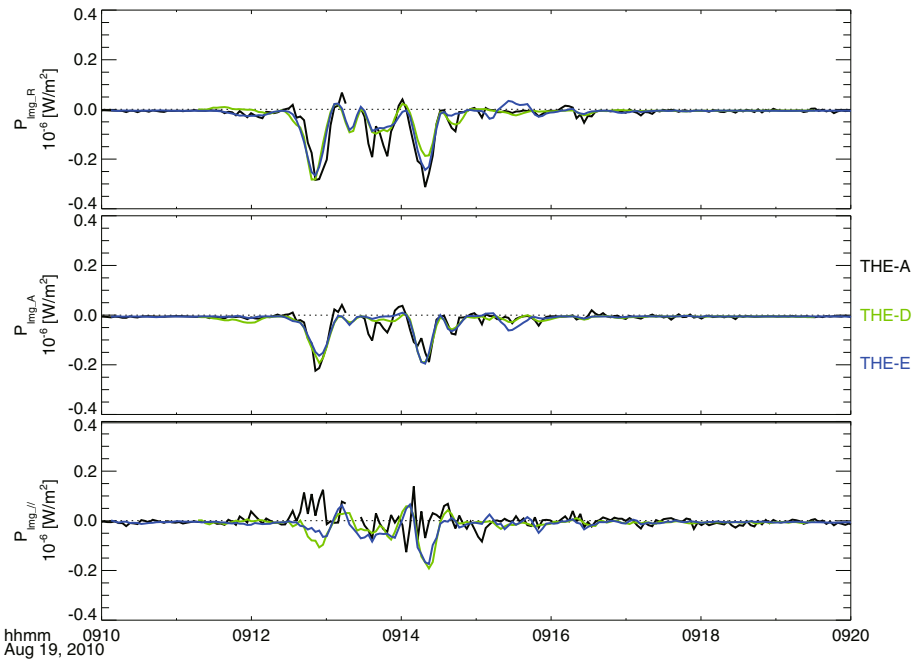

Fig. 6 Poynting flux in the radial (*bottom*), azimuthal (*middle*), and compressional (*bottom*) components associated with the Pi2 pulsations observed by the THEMIS satellites on August 19, 2010

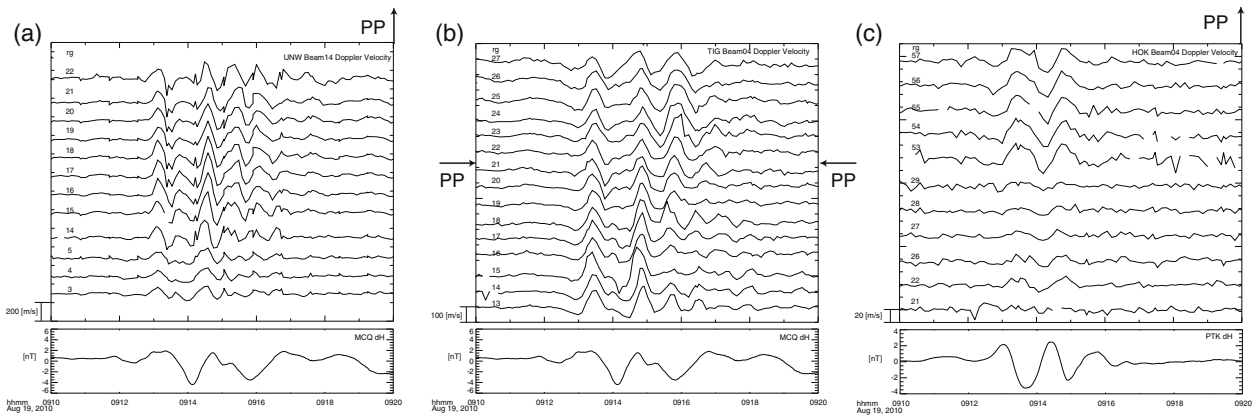

Fig. 7 Time series of Doppler velocities from **a** beam 14 at ranges 3–5 and 14–22 for UNW, **b** beam 4 at the range 13–27 for TIG, and **c** beam 4 at ranges 21–29 and 52–57 for HOK in the *upper panels*, and the magnetic field data in the d*H* component at **a** and **b** MCQ and **c** PTK in the *bottom panels*. The *arrows* indicated the locations of the plasmasphere

(range of 13–18) after 09:15 UT. In the Doppler velocities from both the UNW and TIG radars, Pi2 pulsations followed those at MCQ. Waveforms of Doppler variations from the UNW and TIG radars were quite different from those at MCQ.

Figure 8a–c shows the corresponding power spectral densities $S(f)$ for Doppler velocity variations (dV), as shown in Fig. 7a–c. The plasmapause locations are identified by black arrows. The spectra of dV from the HOK radar, which exhibited echoes at a lower latitude than the UNW and TIG radars, showed a dominant peak at approximately 14 mHz with a maximum power density near the range of 53. In comparison, two dominant spectral peaks at f_1 and f_2 appeared in the $S(f)$ of dV from the UNW radar, as shown in Fig. 8a. The $S(f)$ of dV from beam 14 of the UNW radar exhibited a dominant peak at 24 mHz, which reached a maximum power at a range of 16, and a smaller peak at 11 to 14 mHz, which archived maximum power at lower latitudes in the range of 5. The amplitudes of the 24-mHz signal in the range of 14–22 for the UNW radar were much larger than those of the 11- to 14-mHz and 24-mHz signals for the HOK and TIG radars. The 11- to 14-mHz signal exhibited maximum power in the range of 15 for the TIG radar, whereas the 23- to 24-mHz signal had a smaller or comparable peak to those of other frequencies. The $S(f)$ of dV from the TIG radar at ranges of 23–27 also showed a single peak in the frequency range from 13 to 18 mHz, which was centered at approximately 15 mHz. The $S(f)$ shapes of dV from the TIG radar at ranges of 23–27 were different from those of TIG at ranges of 13–18, which had double peaks at f_1 and f_2. These features indicate that Pi2 pulsations observed at ranges of 23–27 for the TIG radars, which were located outside the plasmasphere, were excited by different mechanisms from those at lower latitudes in the plasmasphere.

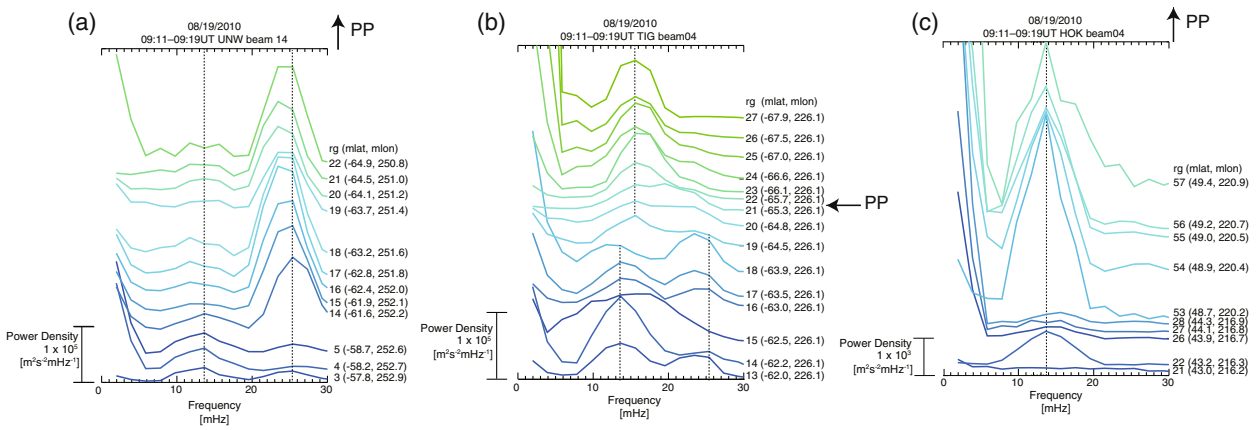

Fig. 8 Power spectral densities of Doppler velocities from **a** beam 14 at ranges 3–5 and 14–22 for UNW, **b** beam 4 at the range 13–27 for TIG, and **c** beam 4 at ranges 21–29 and 52–57 for HOK, as shown in Fig. 7

Figure 9 shows the latitudinal characteristics of the f_1 and f_2 peaks that appeared in the Doppler velocities of the HOK, UNW, and TIG radars. To identify the location of the latitudinal power peak of the f_2 signal that appeared in the radars, the latitudinal profile for the f_2 peak normalized by the f_1 peak $S(f_2)/S(f_1)$ was plotted, and the results are shown in Fig. 9a. The vertical dashed lines indicate the plasmapause locations. The latitudinal $S(f_2)/S(f_1)$ peaks greater than two in the Doppler data were localized at 61° to 65° AACGM latitude and were located near the plasmapause. However, the $S(f_2)/S(f_1)$ of dV from the TIG radar at 61° to 65° AACGM latitude was much smaller than that from the UNW radar. This could be attributed to the longitudinal difference between the UNW and TIG radars. The HOK radar, which was located at a lower latitude than the other radars, observed $S(f_2)/S(f_1)$ to be less than two. Figure 9b, c shows the latitudinal profile for the cross-phase between dV from radars and dH at MMB with high coherence (>0.7) between dV and dH at f_1 and f_2, respectively. The latitudinal phase profiles at both f_1 and f_2 exhibited changes at 55° AACGM latitude. At lower latitudes, the cross-phase was approximately 180° at both f_1 and f_2, whereas at higher latitudes, the cross-phases were between 0° and 90° (around 90°) at f_1 (f_2).

Ground observations

Figure 10a, b shows the geomagnetic field data in the H and D components on the ground from 09:08 to 09:23 UT. The bottom two panels show the geomagnetic field data in the Southern Hemisphere. All ground stations except for Dumont d'Urville (DRV) were located in the plasmasphere. The waveforms of Pi2 pulsations at MQR and DRV were different from those in both the H and D components at MMB, PTK, and Magadan (STC), which were located in the plasmasphere, whereas Pi2 pulsations in the H component at MMB, PTK, and STC oscillated with the same periods and with a slight phase difference.

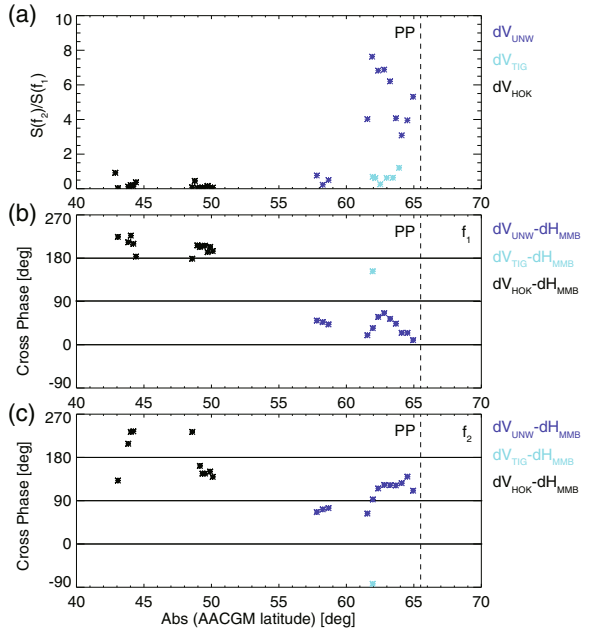

Fig. 9 a Absolute AACGM latitudinal distribution of normalized power, which was defined as $S(f_2)/S(f_1)$, and the cross-phase between the Doppler velocity and dH component of MMB at **b** f_1 and **c** f_2

Figure 11 shows the spectrum densities of the geomagnetic field in the dH and dD components. The power spectra at MMB, PTK, and STC had clear peaks in the frequency range from 9 to 18 mHz, and peaks were centered at approximately 14 mHz. However, the frequency of peaks in the dH component at MCQ was slightly different from those at lower latitudes. Moreover, the frequency of Pi2 pulsations at DRV was much lower than those at lower latitudes. These spatial characteristics of frequencies indicate that the Pi2 pulsations inside the plasmapause were excited by the same source, whereas those outside or close to the plasmapause were excited by different sources.

Discussion

We investigated the spatial characteristics of Pi2 pulsations from data obtained simultaneously by the mid-latitude SuperDARN radars, THEMIS satellites, and ground stations, which were located along the 210° magnetic meridian on the nightside. Our observational results can be summarized as follows:

1. The THA, THD, and THE satellites, which were located in the nightside plasmasphere, observed Pi2 pulsations in the compressional component of the magnetic field (d$B_{//}$) and in the radial and azimuthal components of the electric field (dE_R and dE_A, respectively) with dominant frequencies of approximately 12 to 14 mHz (f_1, fundamental) and 23 to 25 mHz (f_2, second harmonic) with almost identical waveforms as the Pi2 pulsations in the H component (dH) at a low-latitude ground station.
2. The cross-phases of Pi2 pulsations in the d$B_{//}$ and dE_R (dE_A) components relative to the dH component at low latitude were 0° (180°) at both f_1 and f_2.
3. The Poynting flux derived from the electric and magnetic field data of the satellites indicated that the energy of Pi2 pulsations propagated duskward and earthward.
4. All radars observed Doppler dV with multiple dominant frequencies of f_1 and f_2 at latitudes lower than the ionospheric projection of the plasmapause.

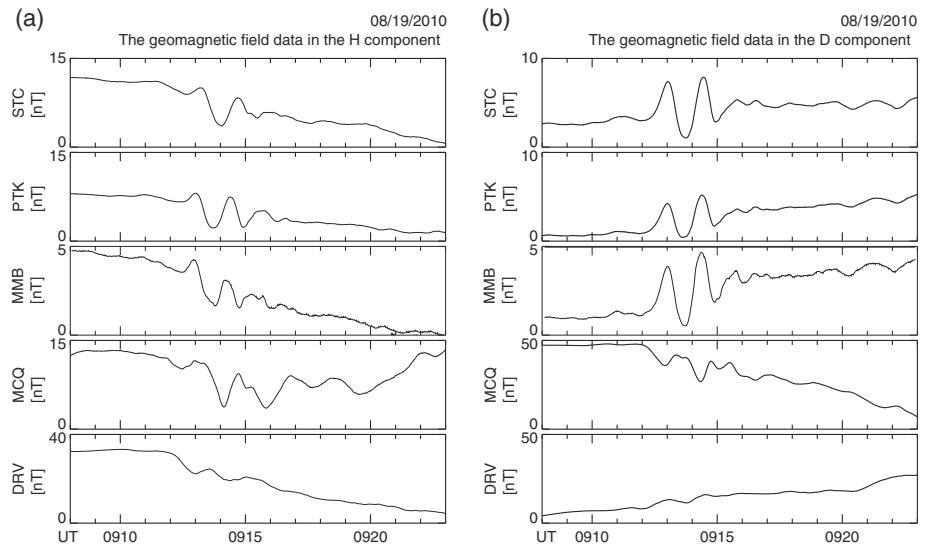

Fig. 10 Time series of geomagnetic field data in **a** the *H* component and **b** the *D* component at high and low latitudes along almost the same meridian as the radar observations

5. Outside the plasmapause, d*V* from the TIG radar had a dominant frequency of 15 mHz.
6. The power of Pi2 pulsations at f_2 from the UNW radar was maximized at 61°–65° AACGM latitude near the plasmapause.
7. The d*V* cross-phase relative to the low-latitude d*H* component was 180° for both f_1 and f_2 at lower latitudes and 0°–90° (around 90°) for f_1 (f_2) at higher latitudes in the plasmasphere.
8. The ground stations observed Pi2 pulsations with frequencies of f_1 and f_2 over a wide range of L in the plasmasphere, whereas Pi2 pulsations appeared outside the plasmapause with frequencies lower than either f_1 or f_2.

In this section, we compare the results of the present study with those of previous studies of mid-latitude Pi2 pulsations and discuss the generation mechanisms of Pi2 pulsations based on this case study.

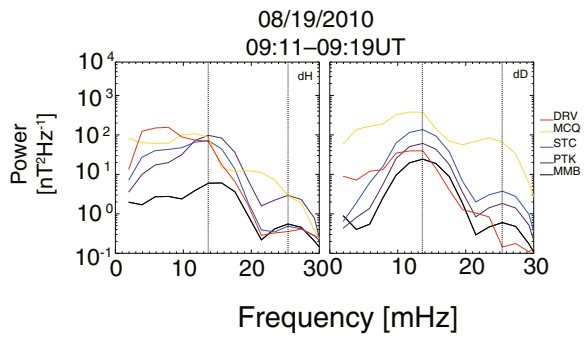

Fig. 11 Power spectral density of the (*left*) d*H* and (*right*) d*D* components of the geomagnetic field data on the ground

Latitudinal observations obtained with mid-latitude SuperDARN radars near the ionospheric projection of the plasmapause can provide new information on the frequency of Pi2 pulsations around the plasmapause. Spectral properties of Doppler velocity variations from the radars revealed that plasmaspheric Pi2 pulsations observed on August 19, 2010, in the Doppler velocity data had common dominant frequencies of approximately 12 to 14 mHz (f_1) and 23 to 25 mHz (f_2). While Pi2 pulsations at both f_1 and f_2 were excited over a wide range in the plasmasphere, Doppler velocity perturbations from the TIG radar at ranges of 23–27 with a frequency of 15 mHz were localized outside the plasmasphere. The localized perturbations on the nightside for $4 < L < 7$ were reported as transient toroidal waves (TTWs) by Takahashi et al. (1996) and Nosé et al. (1998) and quasi-periodic oscillations (QPOs) by Saka et al. (1996). The TTWs (QPOs) are generated by standing Alfvén waves on individual magnetic field lines associated with substorm onsets. Based on the Polar satellite observations, Keiling et al. (2003) demonstrated that TTWs appear outside the plasmasphere. Their results are consistent with the localized perturbations at 15 mHz in our study. Fujita et al. (2002) described the transient behavior of magnetohydrodynamic (MHD) perturbations in the inner magnetosphere from the liner MHD-wave simulations. By using a magnetic model comprised of a dipole magnetic field, the plasmasphere, the ionosphere with Pedersen conductivity, and a free outer boundary, they employed an impulsive eastward magnetospheric current, which was localized at $L = 10$ around the magnetic

equator with a 2-h longitudinal extent around midnight, as a driver of Pi2 pulsations while assuming the substorm current wedge. The liner MHD-wave simulations demonstrated that localized toroidal-mode waves, which are dominant in the magnetic azimuthal and electric radial components, appear simultaneously on the plasmapause and coupled to the poloidal mode when global-mode waves are excited in the poloidal component in the plasmasphere. Because of the wave coupling, localized perturbations appeared in the Doppler velocity data obtained by the TIG radar; although beam 4 of the radar pointing poleward could not observe east–west plasma motions in the ionosphere, which were associated with toroidal waves with the electric field in the north–south component of the ionosphere. Our observations indicate that localized perturbations at 15 mHz were excited at higher latitudes outside the plasmasphere by the coupling TTWs when Pi2 pulsations at f_1 and f_2 were simultaneously excited in the plasmasphere by the global mode.

Although power spectra of Pi2 pulsations in the magnetic and electric field data and Doppler velocity data showed double-peak structures at f_1 and f_2, only Doppler variations obtained by the mid-latitude UNW and TIG radars showed that the power of the f_2 signal was greater than that of the f_1 signal. The localized f_2 power enhancement observed by the UNW radar can be explained by the harmonic structure of Pi2 pulsations, as suggested in Takahashi et al. (2003b). They showed the radial profile of the fundamental and second harmonics of the cavity mode resonance by using magnetic and electric field data from the CRRES satellite. In Fig. 12, which was adapted from Figure 1 of Takahashi et al. (2003b), a two-dimensional box-shaped magnetosphere for the cavity mode resonance was considered wherein the magnetic field was (i) straight and uniform, (ii) directed along the z-axis, and (iii) fixed to the northern and southern boundaries (ionosphere) of the box. Moreover, the field lines at the inner and outer boundaries were fixed. Takahashi et al. (2003b) assumed that the mode is generated between rigid boundaries, namely, the inner boundary of the ionosphere (L_{b1}) and the outer boundary of the plasmapause (L_{b2}). For both harmonic modes, a node of E_A and an antinode of $B_{//}$ were located at these boundaries, where the amplitudes of E_A and $B_{//}$ had a minimum and a maximum, respectively. The radial structure of the harmonic cavity mode had three nodes or antinodes (labeled L_{n1}, L_{n2}, and L_{n3}) between the two boundaries. For the fundamental mode, E_A and $B_{//}$ had an antinode and a node at L_{n2}, at which the second-harmonic E_A and $B_{//}$ had a node and an antinode, respectively. For the second-harmonic mode, there were two further nodes (antinodes) of $B_{//}$ (E_A) at L_{n1} (located between L_{b1} and L_{n2}) and at L_{n3} (located between L_{n2} and L_{b2}). Considering realistic plasma and magnetic field models, the nodes (antinodes) of both the fundamental and second harmonics at L_{n1}, L_{n2}, and L_{n3} were located closer to L_{b2}. In reality, the antinodes of the second-harmonic Pi2 pulsations in the E_A component at L_{n1} and L_{n3} are confined in the small region near the plasmapause. From the THEMIS observations shown in Fig. 3, the outer boundary of the projection plasmapause was located at 65.5° AACGM latitude in the ionosphere. The latitudinal structure of power at the second-harmonic frequency with respect to the fundamental power observed from the UNW radar was largest between 60° and 65° AACGM latitudes close to the plasmapause, whereas the spectrum of Pi2 pulsations observed at lower latitudes by the HOK radar was enhanced at the fundamental frequency. These latitudinal profiles of power were consistent with the radial profile of the harmonic cavity mode structure confined by the plasmapause.

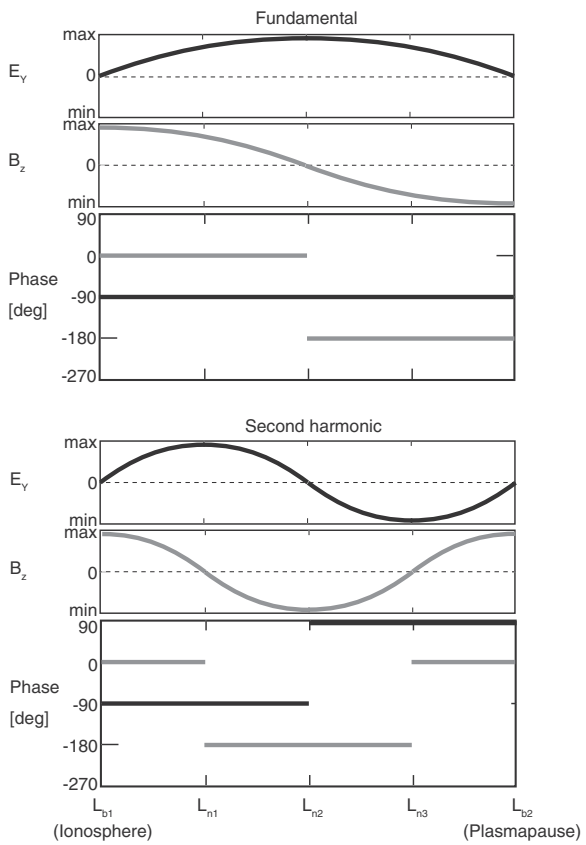

Fig. 12 Radial profiles of phase and amplitude in the identical harmonic cavity mode resonance, which were adapted from Figure 1 of Takahashi et al. (2003b)

As shown in Fig. 9a, the f_2 power observed by the UNW radar was largest at 60°–65° AACGM latitude, which was close to the plasmapause, although the power of the f_2 signals was much smaller than that of the f_1 signals at the nearby MCQ ground station in Fig. 11.

Moreover, the mismatch of spectral shapes between ground magnetometers and radars was reported by Ponomarenko and Waters (2013). The existence of the f_2 signal enhancement not at MCQ, but rather in the radar, might be explained by the spatial coverage of the instruments. The radar can detect ULF waves in the ionosphere with much better spatial resolution for the 45-km range gate cell along the line of sight (LOS). Since the ground magnetometer integrates the signal from a much larger area of the ionosphere, the ground magnetometer could have superimposed signals in a larger area, wherein the f_1 peak enhancement would be larger than that of the f_2 peak. Therefore, the f_2 signal enhancement can be detected only by radars because of their higher spatial resolution.

Another key feature for harmonic cavity mode resonance is the radial (latitudinal) profile of the cross-phase. By using data from the CRRES satellite in the plasmasphere, Takahashi et al. (2003b) presented the radial profile of the E_A-H and $B_{//}$-H cross-phases, while assuming that $B_{//}$ at L_{b1} was in-phase with the H component measured on the same magnetic meridian. The fundamental E_A phase relative to H was −90° anywhere between L_{b1} and L_{b2}, whereas the second-harmonic E_A-H phase was −90° between L_{b1} and L_{n2} and 90° between L_{n2} and L_{b2}. As shown in Fig. 9b, the latitudinal profile of the V-H cross-phase, which corresponds to the E_A-H cross-phase, was 0°–90° at higher latitudes and was out of phase at lower latitudes. The latitudinal profile of the V-H phase was inconsistent with the cavity mode resonance. In addition, the E_A-H cross-phase of 180° at f_1 and f_2 from our satellite observations in the plasmasphere did not provide support for the cavity mode model, in which Pi2 pulsations in the E_A component were ±90° out of phase with those in the H component at low latitudes. In contrast to the E_A component, the $B_{//}$-H cross-phase of 0° at f_1 and f_2 for THA, THD, and THE in this study was consistent with the observations of Takahashi et al. (1995, 2003b). The $B_{//}$-H, E_A-H, and E_R-H phase properties imply that the compressional waves propagate duskward and earthward in the plasmasphere, which was also confirmed by the Poynting flux shown in Fig. 6. These propagating waves have never been reported for magnetic and electric data obtained in the plasmasphere by satellites.

To investigate whether Pi2 pulsations propagate, we estimated the phase velocity from the cross-phase between the Pi2 pulsations in the compressional component from THA and THD at f_1 and f_2, which is equivalent to the time delay between Pi2 pulsations. After $dB_{//}$ from THD was linearly interpolated and resampled at the same 3-s time rate as $dB_{//}$ from THA, we applied FFT to $dB_{//}$ in the time interval from 09:11 to 09:19 UT, and three-point smoothing was conducted in the frequency domain. We derived the coherence and cross-phase between THA and THD. The cross-phases of THD relative to THA were −15.2° and 15.7° at f_1 and f_2, respectively, at which the coherence was perfect (approximately 1). The velocities of −1329 km/s and 2424 km/s were derived from the cross-phases and the radial distance between THA and THD (approximately 4121 km). This result indicates that the wave fronts do not propagate radially because the derived velocities are much larger than the Alfvén speed in the plasmasphere in the magnetic equatorial plane (Moore et al. 1987). We also estimated the azimuthal velocities of Pi2 pulsations from the cross-phase between the Doppler velocity variations observed at almost the same latitudes on beam 14 at the range of 15 from UNW (AACGM Mlat −61.9° and Mlon 252.1°) and on beam 4 at the range of 13 from TIG (AACGM Mlat −62.0° and Mlon 226.1°). We applied FFT to dV in the interval from 09:11 to 09:23 UT (128 data points). The power spectra of dV from TIG and UNW and TIG coherence and the cross-phase relative to UNW were derived. The cross-phases of TIG relative to UNW were 113.6° and 191.7° at f_1 and f_2, respectively, at which the power showed peaks and the coherence was high (approximately 1). The wave fronts of Pi2 pulsations propagated at 56.2 and 63.3 km/s westward in the ionosphere, which correspond to 590 and 650 km/s duskward propagations in the plasmasphere. By using electric and magnetic field data from THEMIS in the inner magnetosphere and low-latitude ground magnetic field data from two stations, Kwon et al. (2012) reported longitudinal variations of Pi2 pulsations associated with fast-mode waves at midnight. Their observations suggest that the Pi2 wave energy is lost as it propagates azimuthally from a source region localized longitudinally. They also suggested that the azimuthal-mode structure takes a longer time to develop than the radial-mode structure because the azimuthal scale size is longer than the radial and north–south length scales in a dipole-like system. The Poynting flux properties from the THEMIS satellite and westward wave front propagations in this study might be explained by duskward propagating waves from the plasmaspheric cavity mode resonance, which is localized at midnight and has a harmonic structure, with energy leaking earthward and duskward.

The alternative generation mechanism for mid-latitude Pi2 pulsations is a BBF-driven model, wherein periodical BBFs propagating earthward from the magnetotail cause periodic pressure pulses in the inner magnetosphere and generate Pi2 pulsations on the ground. If BBFs generate Pi2 pulsations, both the waveform and the frequency content should be similar between Pi2 pulsations in the plasma flow data in the magnetotail on the nightside and ground magnetometer data on the flankside (Kepko and Kivelson 1999; Kepko et al. 2001). However, in this study, we could not confirm that the Pi2 pulsations were generated by BBFs because there were no observations

in the magnetotail. We were able to, however, evaluate the generation mechanisms by latitudinal variations of the waveforms and the dominant frequency of Pi2 pulsations on the ground and from radars. As shown in Fig. 8, Pi2 pulsations in dV with the dominant frequencies of f_1 and f_2 were confined in the plasmasphere, whereas the dominant frequency, which was observed outside the plasmasphere by the TIG radar, was different from f_1 and f_2. In addition, the dominant frequencies of Pi2 pulsations at DRV, which was located on the ground at the highest latitude, were also different from those observed by the mid- and low-latitude ground stations in the plasmasphere (Fig. 10). The results of this study indicate that Pi2 pulsations inside and outside the plasmasphere were not generated by common sources, such as periodic BBFs in the magnetotail. Therefore, we did not use the BBF-driven Pi2 model as a generation mechanism for our observations.

Recently, Pi2 pulsations have been associated with high-speed plasma flows in the plasma sheet besides BBFs. By using data from the THEMIS satellite and a ground magnetometer, Keiling (2012) presented ballooning-mode plasma perturbations propagating westward in the near-Earth plasma sheet around 9 to 12 R_E when westward-traveling Pi2 pulsations appeared simultaneously at high latitudes (>60° magnetic latitude) at the conjugate ground station. They proposed that Pi2 pulsations at high latitudes are generated by the ballooning mode. Auroral observations from the ground and Pi2 magnetic disturbances from THEMIS satellites in the near-Earth plasma sheet region showed that most of the wavelike bright spot structure in the aurora moved westward with large azimuthal wave numbers and the movements of the structure were associated with the phase velocities of Pi2 disturbances, thus providing support for the ballooning instability as Pi2 pulsations arrived at high latitudes (Chang and Cheng 2015). Fujita and Tanaka (2013) considered the scenario of Pi2 pulsations at high and low latitudes by investigating the plasma disturbances in the global MHD model of Tanaka et al. (2010) instead of Pi2 signals in the magnetic field. In the model, they proposed that the SCW could not be regarded as the source of Pi2 pulsations in the inner magnetosphere because it was not reproduced. Instead of the SCW, the high-speed earthward flow in the plasma sheet at the substorm onset suddenly stopped in the ring current region, in which the ambient magnetic field intensity increased. Then, the inner magnetosphere suddenly compressed. The sudden compression invoked a compressional MHD wave propagating in the inner magnetosphere, which have generated cavity mode resonance. They also suggested that the ballooning instability might trigger Pi2 pulsations. To investigate whether Pi2 pulsations at mid and low latitudes are associated with ballooning-mode Pi2 pulsations at high latitudes and the SCW, further investigations over a wider range in the magnetosphere will be required.

Summary

In this study, we compared Pi2 pulsations that were observed simultaneously along almost the 210° magnetic meridian on the duskside during a substorm onset at 09:10 UT on August 19, 2010; the data were obtained from the three Asian-Oceanian SuperDARN radars (Unwin, Tiger, and Hokkaido radars), three THEMIS satellites (THA, THD, and THE), and low- and high-latitude ground stations. All three THEMIS satellites, which were located in the plasmasphere, observed Pi2 pulsation in the compressional magnetic and the radial and azimuthal electric fields. Based on the Poynting flux estimated from the magnetic and electric field measurements, the Pi2 energy propagated earthward and duskward. We compared the power spectral densities, $S(f)$, of Pi2 pulsations and found that they experienced peaks at 12 to 14 mHz (f_1) and 23 to 25 mHz (f_2) in the plasmasphere. We also investigated the latitudinal profile of $S(f_2)/S(f_1)$ in the Doppler velocity (dV) from all radars and the dV cross-phase relative to the dH component at the low-latitude ground station MMB. The $S(f_2)/S(f_1)$ was largest at 21:00 MLT near the plasmapause, which was estimated from the electron number density derived from the THEMIS satellites. While the cross-phases at the lower latitude (<55°) clustered around 180° at both f_1 and f_2, the cross-phase at the higher latitude (>55°) was distributed between 0° and 90° (around 90°) at f_1 (f_2). We conclude that Pi2 pulsations were generated by the compressional waves propagating duskward from the source region in the midnight plasmasphere.

Competing interests

The authors declare that they have no competing interests.

Authors' contributions

MT conducted these studies, participated in the sequence alignment, and drafted the manuscript. NN, YN, and TN participated in designing the study and coordinating the work; they also helped to draft the manuscript. All authors read and approved the final manuscript.

Acknowledgements

The provisional AL index and Kp index were provided by the World Data Center (WDC) for Geomagnetism, Kyoto. We are grateful to the staff of the Kakioka Geomagnetic Observatory for kindly supplying the high-quality MMB data. The present study was supported by the Global COE Program of Nagoya University through the "Quest for Fundamental Principles in the Universe (QFPU)" project and through a joint research program with the Solar-Terrestrial Environment Laboratory, Nagoya University. We also acknowledge a National Aeronautics and Space Administration (NASA) contract (NAS5-02099) and would like to thank V. Angelopoulos for the use of the data from the THEMIS mission. The authors would also like to thank J. W. Bonnell and F. S. Mozer for the use of the EFI data and K. H. Glassmeier, U. Auster, and W. Baumjohann for the use of the FGM data that was provided by the Technical University of Braunschweig with financial support from the German Ministry for Economy and Technology and the German Center for Aviation and Space (DLR) under contract 50 OC 0302. Lately, we would also like to thank P. Dyson, J. Devlin, and M. Parkinson for operating and providing the data from the TIGER radar.

Author details
[1]Institute of Space and Astronautical Science, Japan Aerospace Exploration Agency, 3-1-1 Yoshinodai, Chuo-ku, Sagamihara, Kanagawa 252-5210, Japan. [2]Institute for Space-Earth Environmental Research, Nagoya University, Furo-cho, Chikusa-ku, Nagoya 464-8601, Japan. [3]Department of Atmospheric and Oceanic Sciences, University of California, Los Angeles, CA 90095-1565, USA. [4]National Institute of Information and Communications Technology, 4-2-1, Nukui-Kitamachi, Koganei, Tokyo 184-8795, Japan.

Received: 13 May 2015 Accepted: 10 January 2016
Published online: 17 February 2016

References

Angelopoulos V, Sibeck D, Carlson CW, McFadden JP, Larson D, Lin RP, Bonnell JW, Mozer FS, Ergun R, Cully C, Glassmeier KH, Auster U, Roux A, LeContel O, Frey S, Phan T, Mende S, Frey H, Donovan E, Russell CT, Strangeway R, Liu J, Mann I, Rae J, Raeder J, Li X, Liu W, Singer HJ, Sergeev VA, Apatenkov S, Parks G, Fillingim M, Sigwarth J (2008) First results from the THEMIS mission. Space Sci Rev 141:453–476. doi:10.1007/s11214-008-9378-4

Baker KB, Wing S (1989) A new coordinate system for conjugate studies at high latitudes. J Geophys Res 94(A7):9139–9143. doi:10.1029/JA094iA07p09139

Bourdillon A, Delloue J, Parent J (1989) Effects of geomagnetic pulsations on the Doppler shift of HF backscatter radar echoes. Radio Sci 24:183–195

Chang T-F, Cheng C-Z (2015) Relationship between wave-like auroral arcs and Pi2 disturbances in plasma sheet prior to substorm onset. Earth Planet Space 67:168

Cheng C-C, Chao J-K, Yumoto K (2000) Spectral power of low-latitude Pi2 pulsations at the 210° magnetic meridian stations and plasmaspheric cavity residences. Earth Planet Space 52:615

Chisham G et al (2007) A decade of the Super Dual Auroral Radar Network (SuperDARN): scientific achievements, new techniques and future directions. Surv Geophys 28:33–109. doi:10.1007/s10,712-007-9017-8

Denton RE, Lee DH, Takahashi K, Goldstein J, Anderson R (2002) Quantitative test of the cavity resonance explanation of plasmaspheric Pi2 frequencies. J Geophys Res 107(A7):SMP-4. doi:10.1029/2001JA000272

Frissell NA, Baker JBH, Ruohoniemi JM, Clausen LBN, Kale ZC, Rae IJ, Kepko L, Oksavik K, Greenwald RA, West ML (2011) First radar observations in the vicinity of the plasmapause of pulsed ionospheric flows generated by bursty bulk flows. Geophys Res Lett 38:L01103. doi:10.1029/2010GL045857

Fujita S, Nakata H, Itonaga M, Yoshikawa A, Mizuta T (2002) A numerical simulation of the Pi2 pulsations associated with the substorm current wedge. J Geophys Res 107(A3):SMP-2. doi:10.1029/2001JA900137

Fujita S, Tanaka T (2013) Possible generation mechanisms of the Pi2 pulsations estimated from a global MHD simulation. Earth Planet Space 65:453–461

Gjerloev JW, Greenwald RA, Waters CL, Takahashi K, Sibeck D, Oksavik K, Barnes R, Baker J, Ruohoniemi JM (2007) Observations of Pi2 pulsations by the Wallops HF radar in association with substorm expansion. Geophys Res Lett 34: L20103. doi:10.1029/2007GL030492

Greenwald RA, Baker KB, Dudeney JR, Pinnock M, Jones TB, Thomas EC, Villain J-P, Cerisier J-C, Senior C, Hanuise C, Hunsucker RD, Sofko G, Koehler J, Nielsen E, Pellinen R, Walker ADM, Sato N, Yamagishi H (1995) DARN/SuperDARN: a global view of the dynamics of high-latitude convection. Space Sci Rev 71: 761–795

Keiling A, Kim K-H, Wygant JR, Cattell C, Russell CT, Kletzing CA (2003) Electrodynamics of a substorm-related field line resonance observed by the Polar satellite in comparison with ground Pi2 pulsations. J Geophys Res 108(A7):1275. doi:10.1029/2002JA009340

Keiling A, Takahashi K (2011) Review of Pi2 models. Space Sci Rev 161:63

Keiling A (2012) Pi2 pulsations driven by ballooning instability. J Geophys Res 117:A03228

Kepko L, Kivelson M (1999) Generation of Pi2 pulsations by bursty bulk flows. J Geophys Res 104(A11):25021–25034. doi:10.1029/1999JA900361

Kepko L, Kivelson MG, Yumoto K (2001) Flow bursts, braking, and Pi 2 pulsations. J Geophys Res 106(A2):1903–1915

Kwon H-J, Kim K-H, Lee D-H, Takahashi K, Angelopoulos V, Lee E, Jin H, Park Y-D, Lee J, Sutcliffe PR, Auster HU (2012) Local time-dependent Pi2 frequencies confirmed by simultaneous observations from THEMIS probes in the inner magnetosphere and at low-latitude ground stations. J Geophys Res 117: A01206. doi:10.1029/2011JA016815

Lin CA, Lee LC, Sun YJ (1991) Observations of Pi 2 pulsations at a very low latitude (L = 1.06) station and magnetospheric cavity resonances. J Geophys Res 96(A12):21105–21113. doi:10.1029/91JA02029

Luo H, Chen GX, Du AM, Angelopoulos V, Xu WY, Zhao XD, Wang Y (2011) THEMIS multipoint observations of Pi2 pulsations inside and outside the plasmasphere. J Geophys Res 116:A12206. doi:10.1029/2011JA016746

Moore T, Gallagher DL, Horwitz JL, Comfort RH (1987) MHD wave braking in the outer plasmasphere. Geophys Res Lett 14:1007

Nosé M, Iyemori T, Nakabe S, Nagai T, Matsumato H, Goka T (1998) ULF pulsations observed by the ETS-VI satellite: Substorm associated azimuthal Pc4 pulsations on the nightside. Earth Planet Space 50:63–80

Nosé M (1999) Automated detection of Pi2 pulsations using wavelet analysis: 2. An application for dayside Pi2 pulsations study. Earth Planet Space 51:23

Ponomarenko PV, Menk FW, Waters CL (2003) Visualization of ULF waves in SuperDARN data. Geophys Res Lett 30:1926. doi:10.1029/2003GL017757

Ponomarenko PV, Waters CL (2013) Transition of Pi2 ULF wave polarization structure from the ionosphere to the ground. Geophys Res Lett 40:1474–1478. doi:10.1002/grl.50271

Saito T, Matsushita S (1968) Solar cycle effects on geomagnetic Pi 2 pulsations. J Geophys Res 73(1):267–286. doi:10.1029/JA073i001p00267

Saka O, Akaki H, Watanabe O, Baker DN (1996) Ground-satellite correlation of low-latitude Pi2 pulsations: a quasi-periodic field line oscillation in the magnetosphere. J Geophys Res 101:15433–15440

Takahashi K, Ohtani S, Anderson BJ (1995) Statistical analysis of Pi 2 pulsations observed by the AMPTE CCE spacecraft in the inner magnetosphere. J Geophys Res 100(A11):21929–21941. doi:10.1029/95JA01849

Takahashi K, Anderson BJ, Ohtani S-I (1996) Multisatellite study of nighttime transient toroidal waves. J Geophys Res 101:24815–24825

Takahashi K, Lee D-H, Nose' M, Anderson RR, Hughes WJ (2003a) CRRES electric field study of the radial mode structure of Pi2 pulsations. J Geophys Res 108(A5):1210. doi:10.1029/2002JA009761

Takahashi K, Anderson RR, Hughes WJ (2003b) Pi2 pulsations with second harmonic: CRRES observations in the plasmasphere. J Geophys Res 108(A6): 1242. doi:10.1029/2003JA009847

Tanaka T, Nakamizo A, Yoshikawa A, Fujita S, Shinagawa H, Shimazu H, Kikuchi T, Hashimoto KK (2010) Substorm convection and current system deduced from the global simulation. J Geophys Res 115:A05220. doi:10.1029/2009JA014676

Teramoto M, Nishitani N, Pilipenko V, Ogawa T, Shiokawa K, Nagatsuma T, Yoshikawa A, Baishev D, Murata KT (2014) Pi2 pulsation simultaneously observed in the E and F region ionosphere with the SuperDARN Hokkaido radar. J Geophys Res 119:3444–3462. doi:10.1002/2012JA018585

Tsyganenko NA (1996) Effects of the solar wind conditions on the global magnetospheric configuration as deduced from data-based field models. In: Rolfe E, Kaldeich B (eds) Third International Conference on Substorms (ICS-3) Eur Space Agency Spec Publ, ESA SP-389., pp 181–185

Yeoman TK, Orr D (1989) Phase and spectral power of mid-latitude Pi 2 pulsations: evidence for a plasmaspheric cavity resonance. Planet Space Sci 37:1367–1383. doi:10.1016/0032-0633(89)90107-4

Yeoman TK, Lester M, Milling DK, Orr D (1991) Polarization, propagation and MHD wave modes of Pi2 pulsations: SABRE/SAMNET results. Planet Space Sci 39(7):983